Published in final edited form as:
J Immunol. 2010 May 1; 184(9): 5333–5343. doi:10.4049/jimmunol.0903382.

IFNγ promotes complement expression and attenuates amyloid plaque deposition in APP transgenic mice

Paramita Chakrabarty[*], **Carolina Ceballos-Diaz**[*], **Amanda Beccard**[*], **Dennis Dickson**[*], **Todd E. Golde**[*,1], and **Pritam Das**[*]

[*]Department of Neuroscience, Mayo Clinic, 4500 San Pablo Rd, Jacksonville, FL-32224

Abstract

Reactive gliosis surrounding amyloid β (Aβ) plaques is an early feature of Alzheimer's disease (AD) pathogenesis and may signify activation of the innate immune system in an attempt to clear or neutralize Aβ aggregates. In order to evaluate the role of IFNγ mediated neuroinflammation on the evolution of Aβ pathology in transgenic mice, we have expressed murine IFNγ (mIFNγ) in the brains of amyloid β precursor protein (APP) transgenic mice using recombinant adeno-associated virus serotype 1. Expression of mIFNγ in brains of APP TgCRND8 mice results in robust non-cell autonomous activation of microglia and astrocytes, and significant suppression of Aβ deposition. mIFNγ expression had no significant effects on APP levels, APP processing or steady state Aβ levels *in vivo*. On the other hand, mIFNγ expression upregulated MHCII and CD11c levels and early components of the complement cascade *in vivo*. Taken together, these results suggest that mIFNγ expression in the brain suppresses Aβ accumulation through synergistic effects of reactive gliosis and complement activation by promoting opsonization and phagocytosis of Aβ aggregates.

Keywords

Amyloid β; IFNγ; Neuroinflammation; complement; recombinant adeno-associated virus

Introduction

Alzheimer's disease (AD), the most common form of cognitive dementia, is a progressive neurodegenerative disorder. The neuropathological hallmarks of AD, extracellular fibrillar aggregates of amyloid β (Aβ) in senile plaques, intracellular tau neurofibrillary tangles and neurodegeneration, are associated with induction of chronic neuroinflammation (1). Senile plaque associated neuroinflammation occurs early in the disease process in humans and is recapitulated in amyloid β precursor protein (APP) transgenic mice brains (2, 3). Several lines of evidence suggest that Aβ aggregates directly induce neuroinflammation resulting in neurotoxicity. Aggregated Aβ activates microglia in culture by binding to the receptor for advanced glycation endproducts (4) as well as to different scavenger receptors (5, 6). Such interactions have been reported to be exacerbated by interactions with microglial costimulatory factors like CD14 and CD40 ligand (7, 8), supporting a close pathologic link between Aβ plaque pathology and the chronic activation of the innate immune system. Such inflammation has been proposed to result in increased oxidative stress, mitochondrial dysfunction, upregulation of amyloidogenic APP processing and increased Aβ deposition

[*]**Correspondence:**das.pritam@mayo.edu; tgolde@ufl.edu, **Phone**: 1-904-953-1086 (PD), 1-904-472-7538 (TEG), **Fax**: 1-904-953-7117.
[1]Present Address: Center for Translational Research in Neurodegenerative Disease, College of Medicine, University of Florida, 1600 SW Archer Road, Gainesville, FL-32608.

(9–13). Conversely, some recent evidence demonstrates that activation of the innate immune response could play a protective role, at least with respect to plaque deposition. Hippocampal expression of IL-1β, a pro-inflammatory cytokine, in APPswe/PS1dE9 mice results in increased microglial activation and subsequent amelioration of plaque pathology (14). Stimulation of the Toll-like receptors have been shown to significantly decrease Aβ burden (15) whereas knocking out TLR2 or TLR4 in APP mice was shown to accelerate Aβ deposition (16, 17).

Neuroinflammation is a well-defined feature of AD pathology, but its role in regulating Aβ deposition remains controversial. Experimental data suggests that glial activation may enhance or suppress Aβ pathology, and that Aβ accumulation may be critically dependent on the factors driving the immune response, as well as the strength and context of the immune response (1, 18). As part of a broader series of studies examining the effects of numerous cytokines and chemokines on Aβ accumulation (19), we have evaluated the effects of murine IFNγ (mIFNγ) on Aβ pathology in APP mice. IFNγ, a pleiotropic cytokine, is a critical component of the innate immune response against viral and intracellular bacterial infections and in tumor control (20). IFNγ is the hallmark cytokine secreted by Th1 cells, dendritic cells and NK cells (21). It is a potent activator of both microglia and astrocytes in the central nervous system (CNS) via upregulation of MHCII antigen and is associated with establishment of the antigen presenting phenotype (APC) (21). Though IFNγ levels are not reported to be increased in AD, many IFNγ responsive genes are upregulated in the AD brain (22, 23). IFNγ levels have been shown to be increased in APP transgenic mice (24–26). Current studies do not demonstrate a clear role for IFNγ with respect to Aβ deposition phenotypes. Deletion of the IFNγ receptor in APP transgenic mice has been reported to decrease Aβ plaque burden via inhibiting IFNγ mediated pathogenic APP processing (13), consistent with *in vitro* studies showing that IFNγ enhances amyloidogenic APP processing via the β- and γ-secretases (27). Human IFNγ also leads to increased intracellular Aβ accumulation in mutant APP/tau/PS1 triple transgenic mice with no changes in APP levels (28). On the other hand, low doses of IFNγ were reported to clear Aβ plaques *in vivo* by T cell dependent mechanisms (29) and improve learning in APP transgenic mice (30).

To further explore the role of IFNγ in regulating Aβ accumulation, we have used recombinant adeno-associated virus serotype 1 (rAAV1) to express murine IFNγ (mIFNγ) in the brains of APP transgenic TgCRND8 mice. rAAV1-mIFNγ over-expression led to widespread non-cell autonomous activation of glia and upregulation of MHCII and CD11c. mIFNγ expression was accompanied by a significant decrease in Aβ plaque burden with no alterations in steady state Aβ levels, APP processing or APP protein levels. Complement system components C1q, C3 and C4a were significantly upregulated in mIFNγ expressing APP mice compared to control mice. Taken together, these results provide clear evidence that mIFNγ attenuates Aβ accumulation *in vivo*, and this effect is likely mediated by synergistic activation of glia and the complement system that enhances Aβ aggregate phagocytosis and clearance.

Materials and Methods

Mice

All animal husbandry procedures performed were approved by the Mayo Clinic Institutional Animal Care and Use Committee in accordance with National Institutes of Health guidelines. To generate CRND8 mice, male TgCRND8 mice containing a double mutation in the human APP gene (KM670/671NL and V717F) (31) were mated with female B6C3F1/Tac mice (Harlan). Hemizygous male Tg2576 mice (32) expressing mutant human APP (KM670/671NL) gene were mated with female B6SJLF1 mice (Jackson Laboratories). All

animals were housed three to five to a cage and maintained on *ad libitum* food and water with a 12 hr light/dark cycle

rAAV1 construction and preparation

mIFNγ was cloned in pAAV vector from Image clone 8733812 (Open Biosystem). mTNFα was cloned in pAAV vector from Image clone 40126376 (Open Biosystem). pAAV-EGFP is a kind gift from M. During (Ohio State University). rAAV1 viruses expressing mIFNγ, EGFP or TNFα, under the control of the cytomegalovirus enhancer/chicken β actin promoter were generated by calcium-phosphate transfection of pAM/CBA-pI-WPRE-BGH, rAAV1 cis-plasmid pH21 (rAAV1 helper plasmid), and pF6 into a HEK293 cell line. 48 hr after transfection, cells were lysed in the presence of 0.5% sodium deoxycholate and 50 U/ml benzonase (Sigma) by repeated rounds of freeze/thaws at –80°C and 37°C. The virus was isolated using a discontinuous Iodixanol gradient and then affinity purified on a HiTrap HQ column (GE Healthcare). Samples were eluted from the column and buffer exchanged to PBS using an Amicon Ultra 100 Centrifugation device (Millipore). The genomic titer of each virus was determined by Q-PCR using the ABI 7900 (Applied Biosystems).

rAAV1 injection in mice

The injection procedures were performed as described previously (19, 33). Both APP transgenic and non-transgenic TgCRND8 littermates were injected with rAAV1-mIFNγ or rAAV1-EGFP as controls on neonatal day P2 (36–48hrs after birth). Briefly, P2 pups were cryoanesthetized and 2 μl of rAAV1 construct (10^{12} particles/ml) were bilaterally injected into the cerebral ventricle of newborn mice using a 10μl Hamilton syringe with a 30” needle (Hamilton, NV, USA). The pups were placed on a heating pad for recovery and returned to their mother. Mice were euthanized at the end of 5 months for analysis (n=10/group). For Tg2576 mice, P0 pups (<24hrs after birth) were injected in the cerebral ventricles with rAAV1-mIFNγ and rAAV1-EGFP (10^{12} particles/ml) and mice were euthanized after 3 months for analysis (n=6/group).

Stereotaxic Injections in adult TgCRND8 mice

4 month old TgCRND8 mice were injected bilaterally into the hippocampus with rAAV1-mIFNγ or EGFP (10^{13} particles/ml). Mice were anesthetized with 1.5% isoflurane in 1% oxygen and secured into a Kopf apparatus (Model 900 Small Animal Stereotaxic Instrument, David Kopf Instruments). All surgical procedures were performed under aseptic conditions. The scalp was scrubbed with betadine and midline incision made. A burr hole (0.5 mm) was drilled in the skull at –1.7 mm caudal and 1.6 mm lateral from the bregma. A 30” needle mounted to a 10μl syringe (Hamilton) preloaded with virus was lowered 1.2mm from the brain surface. A UMP2 Microsyringe Injector and Micro4 Controller (World Precision Instruments) was used to inject 2μl of virus (10^{12} particles/ml) at a constant rate over 10 minutes. After allowing an additional 10 minutes, the needle was raised slowly. The burr hole was sealed and the scalp incision was closed with surgical staples. Mice were monitored post-surgically and administered analgesics overnight and staples were removed 7–10 days after surgery. Mice were euthanized after 6 weeks for analysis (n=5 for rAAV1-mIFNγ; n = 6 for rAAV1-EGFP)

Real-time Q-PCR

Total RNA from mice brain was isolated using the RNaqueous kit (Ambion) according to the manufacturer's instructions and RNA sample was reverse transcribed using Superscript III (Invitrogen). Dilutions of each cDNA prep were used to assess actin RNA levels, and samples were then adjusted to give equivalent levels of actin per well in subsequent Q-PCRs for other genes. The Q-PCR was performed with the MX4000 unit (Agilent Technologies)

using SYBR Green to detect the amplification products as suggested by the manufacturers. The following cycles were performed: initial denaturation cycle of 95°C for 10 min, followed by 40 amplification cycles of 95°C for 15 s and 60°C for 1 min and ending with one cycle at 25°C for 15 s. Analysis was performed on the data output from the MX4000 software (Agilent Technologies) using Microsoft Excel XP. Relative quantification of mRNA expression was calculated by the ΔC_T methods described by the manufacturer (ABI Prism 7700 Sequence Detection System, User Bulletin #2). Primer sequences for the murine genes were designed from the Roche Universal Probe Library sequence (Hoffman La Roche)

Preparation of brain homogenate for immunoblotting, mIFNγ ELISA and Aβ ELISA assay

Snap-frozen forebrain samples (left hemibrains) were homogenized sequentially in RIPA Buffer and 2% SDS buffer with 1x protease inhibitor mixture (Roche). The homogenate was centrifuged at 100,000×g for 1 h at 4°C at each step. Protein concentration in supernatants was determined using the Bicinchoninic Acid Protein Assay kit (Pierce). Protein samples (20–40μg) were separated on Bis-Tris 12% XT gels (Bio-Rad) with XT-MES buffer and transferred to 0.45μm nitrocellulose membranes. Blots probed with the antibody CT20 (T. E. Golde; anti-APP C-terminal 20 amino acid; 1:1000); 82E1 (IBL; anti Aβ 1–16; 1:1000); Glial Fibrillary Acidic Protein/GFAP (Cell Signaling; 1:1000); cd11b (Novus Biological; 1:500); C3 (Santa Cruz, 1:100) and BACE1 (Clone 3D5; R. Vassar; 1:500). Blots were reprobed with anti β-actin (1:1000; Sigma) as a loading control. Relative band intensity was quantified using ImageJ software (NIH).

mIFNγ levels were evaluated using sandwich capture ELISA assays using RIPA soluble mouse forebrain lysates as per manufacturer's instructions (BD OptiEIA, BD Biosciences). The results were compiled using SoftMax Pro software (Molecular Device).

Biochemical determination of Aβ levels using Aβ sandwich ELISA

For brain Aβ ELISAs from P2 injected transgenic mice, hemi-forebrains (left hemibrain) were sequentially homogenized in RIPA buffer, 2% SDS and 70% formic acid as described before (19). For adult mice injected in the hippocampus, the brains were coronally dissected 1 mm anterior and posterior to the point of injection and used for subsequent analysis. Aβ levels were determined by human Aβ end-specific sandwich ELISAs as previously described (33): for Aβ42 - capture with mAb 2.1.3 (human Aβx-42 specific) and detection with HRP-conjugated mAb Ab9 (human Aβ1–16 specific); for Aβ40 - capture with mAb Ab9 and detection with HRP-conjugated mAb 13.1.1 (human Aβx-40 specific). Detection of endogenous mouse Aβ40 was done using Diethyl Amine extracted brains of 5 month old nontransgenic mice injected at P2. For detection of endogenous mouse Aβ, antibody 32.4.1 (rodent Aβ1–16 specific) was used for capture followed by HRP-conjugated mAb 13.1.1 antibody for detection. The results were analyzed using SoftMax Pro software (Molecular Device).

Immunohistochemical Imaging and Image Processing

At various timepoints during the study, mice were sacrificed and the right hemibrain was fixed in 4% paraformaldehyde overnight. For P2 injected mice, sagittal sections initiating from the midline were used for analysis. For adult mice injected in the hippocampus, the brain was coronally dissected at the point of injection and used for subsequent analysis. Paraffin embedded sections (6μm thick) were immunostained using the following primary antibodies and the Dako Envision Plus visualization system: Aβ antibody 33.1.1 (1:1500, human Aβ1–16 specific); Aβ42 antibody 2.1.3 (1:1000; human Aβ42 specific); Aβ40 antibody 13.1.1 (1:1000; human Aβ40 specific); anti-GFAP (1:1000, Sigma); anti-Ionized calcium-binding adaptor molecule 1/Iba-1 (1:1000, Wako); anti-EGFP (1:1000; Invitrogen),

anti-CD45 (Chemicon, 1:50), Ly-6C (1:50, Abcam) and anti-C3 (Abcam, 1:100). Nissl stain, Luxol Fast Blue and von Kossa Stain histological stains were performed on paraffin embedded sections according to established procedures. Immunohistochemically stained sections were captured using the Scanscope XT image scanner (Aperio) and analyzed using the ImageScope program. The final images and layouts were created using Photoshop CS2 (Adobe).

Quantification of amyloid deposition

Immunostained total Aβ, Aβ42 and Aβ40 plaque burdens in the forebrain (cortex and/or hippocampus) was calculated using the Positive Pixel Count program available with the Imagescope software (Aperio). At least three sections per brain (n=10/group for the neonatal P2→5 month group and n=5/group for the adult 4→5.5 month group), 30μm apart, were averaged to calculate the plaque burden for each sample. All of the above analyses were performed in a blinded manner.

Hippocampal Cell Count

This was based on the "unbiased brick counting rule" adapted from Howard et al (34). Briefly, paraffin-embedded brain sections were stained with Nissl stain and scanned with ScanScope XT (Aperio Technologies) at a magnification of 400× (n=5/group). The number of cells in a fixed area of interest (a 9000 by 9000 pixel area of the hippocampus) of each sample was counted using Metamorph (Meta Imaging version 7.5.5; Molecular Devices). Ten random blocks of equal size were created, each measuring 300 by 300 Metamorph units and placed randomly within the area of interest. Stained cells touching the left and bottom edges of the blocks were not counted, and cells touching the top and right edges that were equal to or greater than 50% inside the block were counted, as well as all other cells fully placed within the block. The dimensions of the area of interest as well as the individual blocks were maintained constant throughout the analyses. At least three individual sections per sample, 30μm apart, were averaged to calculate the final cell count. All of the above analyses were performed in a blinded manner.

Calculation of Hippocampal Cell Diameter

Using the ImageScope software measurement tool (Metamorph), 30 cells were randomly measured within the same area of interest mentioned above. The cell diameter was defined as the longest axis through the visible cell membrane. Only the cells placed within the same plane of focus was used for measurements in each case. The average of the 30 measurements was taken per slide and then these were further averaged among the three triplicates for each sample.

Phagocytosis Assay with primary mouse glial culture

Microglia were obtained from cerebral cortices of neonate mice (1–2 days old). Isolated cortices were minced and triturated in HBSS containing 50μg/ml DNase I (Sigma). Cells were then resuspended in DMEM High Glucose media in the presence of 25ng/ml GM-CSF (Sigma) to yield a primary mixed neuronal culture. Microglia were shaken off the primary mixed culture after 7 days and plated in a chamber slide system for analysis (Lab-Tek-II slide system, Fisher Scientific) at a concentration of $2–4\times10^5$ cells/ml. Immunocytochemistry with anti Iba-1 (1:250, Wako) was done to assess the purity of isolated microglia. All studies were conducted on cultures in which >95% of cells were positive for Iba-1. CD68 (FA-11, Abcam, 1:200) immunofluorescence was performed on 2% paraformaldehyde (containing 50mM sucrose) fixed glia. Hilyte 568 labeled Aβ42 peptide (Anaspec) was allowed to aggregate by incubating in PBS buffer at 37°C for 6 hr. The aggregated fibrillar Aβ42 (fAβ) was then sonicated (3×10 sec burst) to generate smaller

fibrillar structures (microaggregates) for use in microglial phagocytosis assay. The glial culture in chamber slides was incubated with 200ng/ml of recombinant carrier free mIFNγ (R&D Systems) for 4 hr and then after changing the culture medium, 1.5 μg of sonicated pre-aggregated Aβ42-HilyteFluor 568 was added for 10 min at 37°C. Cells were washed in warm medium and then with sterile PBS, fixed in 2% paraformaldehyde containing 50mM sucrose and mounted in Fluorescent mounting medium containing DAPI (Vector Labs) and visualized under fluorescence. All of the images were captured at the same time using the same exposure time. Unmanipulated fluorescent images were analysed using Metamorph program. The areas of interest defined by a fixed area was used to measure average fluorescence intensity in the "red" channel using an embedded program.

Statistical analysis

Two-way ANOVA with post hoc Holm-Sidak multiple-comparison test or two-tailed Student's t test was used for statistical comparison (SigmaStat 3.0 version). Variability of the estimates was reported as standard error. A p value of less than 0.05 was considered significant. Asterisks in the figures denote statistical significance at $p < 0.05$. All graphical analyses were done using Prism 4 (GraphPad Software).

Results

Intracranial expression of mIFNγ using rAAV1 mediated transduction of the mouse brain

Two paradigms were used to evaluate the effects of rAAV1-mediated expression of mIFNγ on Aβ pathology in APP TgCRND8 mice. The first paradigm investigated the effects of mIFNγ expression initiated prior to the onset of plaque deposition. TgCRND8 mice pups (36–48 hours old; neonatal day P2) were bilaterally injected with rAAV1-mIFNγ or rAAV1-EGFP (control mice) into the cerebral ventricles and analyzed after 5 months (P2→5 month). P2 somatic brain transgenic technique delivery results in expression largely localized in the choroid plexus and ependymal cells lining the ventricles, along with a few neurons in the hippocampus, cortex and cerebellum, as measured by immunohistochemical analysis with anti EGFP antibody (Suppl. Fig 1, A-H). In contrast, injection in P0 mice (0–12 hr old) results in widespread transduction and expression of the transgene in mouse brain (19). In pilot studies, rAAV1-mIFNγ injection on day P0 resulted in lethality, runted litters and general malaise indicating that neonatal P0 delivery of rAAV1-mIFNγ is neurotoxic. In contrast, pilot studies of P2 rAAV1-mIFNγ injections showed that it was well-tolerated; therefore, we generated larger cohorts of P2 injected mice for further investigation.

The second paradigm evaluated the effects of rAAV1-mIFNγ or rAAV1-EGFP delivery to the hippocampus of adult 4 month old TgCRND8 mice. rAAV1-mIFNγ or rAAV1-EGFP was stereotaxically injected into the hippocampus of 4 month-old TgCRND8 mice and mice were sacrificed 6 weeks later (4→5.5 month). Immunohistochemical analysis with anti EGFP antibody shows that the viral transgene is predominantly expressed in the hippocampal CA neurons, parts of the dentate gyrus, neuronal projections in the cortex and some overlying cortical neurons following intrahippocampal delivery of rAAV1-EGFP (Suppl Fig 1, I-L). We have previously shown that rAAV1-EGFP expression has no effect on amyloid pathology or gliosis when compared to non-injected or PBS-injected mice (19, 33). Therefore, rAAV1-EGFP expressing mice were used as the control cohorts in all the paradigms tested in this study.

Expression of mIFNγ in mouse brain induces widespread and striking microgliosis and astrogliosis

Detailed immunohistochemical analysis of the P2→5 month rAAV1-mIFNγ expressing TgCRND8 mice showed extensive microgliosis and astrogliosis, compared to EGFP

expressing control mice. There was a massive increase in both GFAP reactive astrocytes and Iba-1 reactive microglia in these mice (Fig 1, A-L). Widespread Iba-1 positive reactive microglia were seen around the hippocampal CA1 to CA3 region, periventricular areas, frontal cortex, basal ganglia and cerebellum compared to control mice (Fig 1, A-F). Although Iba-1 immunostaining results in detection of all microglia in the brain, the Iba-1 reactive microglia in mIFNγ expressing mice displayed increased hypertrophic processes, indicating a heightened state of activation (Fig 1, F). Quantitation of Iba-1 immunostaining shows a striking increase in microglial immunoreactivity in mIFNγ expressing mice brains compared to controls (Fig 1, M). Similarly, significant numbers of GFAP immunoreactive activated astrocytes displaying hypertrophic processes were seen in the cortex, hippocampus, midbrain and cerebellum of P2→5 month old TgCRND8 mice injected with mIFNγ compared to controls (Fig 1, G-L). Quantitation of GFAP immunoreactivity also indicates a substantial increase in astrocytic activation in mIFNγ expressing mice compared to controls (Fig 1, M). Immunoblot analysis of the microglial activation marker CD11b/ Complement Receptor 3 (CR3) and the astrocytic marker GFAP showed significant increases in both markers in P2→5 month old rAAV1-mIFNγ injected TgCRND8 mice compared to age-matched controls (Fig 1, O-P). Using lysates obtained from the forebrain of P2→5 month mice, we also demonstrate significant increases in mIFNγ protein levels in rAAV1-mIFNγ injected animals compared to rAAV1-EGFP injected control animals (Fig. 1, N), indicating that rAAV1-mIFNγ transduction led to expression and secretion of mIFNγ in the brain.

Focal expression of rAAV1-mIFNγ in the hippocampus (adult 4→5.5 month paradigm) also resulted in robust reactive microgliosis (Suppl. Fig 2, A-F) and astrogliosis (Suppl. Fig 2, G-L) compared to rAAV1-EGFP expressing control mice, especially in and around the hippocampus. Quantification of Iba-1 and GFAP immunoreactivity showed a massive increase in both markers in mIFNγ expressing mice compared to controls (Suppl. Fig 2, M). Additionally, immunoblot analysis also showed significant increases in CD11b/CR3 and GFAP levels in mIFNγ expressing mice compared to age-matched controls (Suppl. Fig 2, O-P). ELISA analysis of mIFNγ levels from RIPA soluble brain lysates (dissected 1 mm anterior and 1 mm posterior to the injection site) confirmed a significant increase in mIFNγ protein levels in rAAV1-mIFNγ injected animals compared to age-matched controls (Suppl. Fig 2, N).

Next, we characterized the pathological attributes of mIFNγ expression in P2→5month APP TgCRND8 transgenic mice. In addition to reactive gliosis, mice expressing mIFNγ developed mineralized deposits in the thalamus and basal ganglia (Suppl. Fig 3, A-B). However, in 4→5.5 month TgCRND8 mice, no calcification was evident, suggesting that this is an age- and dose-dependent effect of mIFNγ in brain (Suppl. Fig 3, C-D). The focal mineralization stained positive with von Kossa indicating presence of calcium (Suppl. Fig 3, E). In all cases examined, the hippocampus and frontal cortex were spared of dystrophic calcification (Suppl. Fig 3, E, inset 1). No peripheral macrophage infiltrates (as assessed by CD45 immunostaining) was apparent (data not shown) or presence of CD3 immunopositive T cells were apparent in the hippocampus and frontal cortex of IFNγ expressing mice (Suppl. Fig 3, F-K). As a positive control for CD3 immunohistochemical reactivity, we included a brain section from a genotype and age matched CRND8 mice injected with rAAV1-TNFα, which shows copious amounts of CD3 immunoreactivity in the brain parenchyma (Suppl. Fig 3, H, K). To determine if IFNγ over-expression affected neuronal viability, we performed image analysis of Nissl stained hippocampal neurons in mIFNγ expressing TgCRND8 mice. Quantification of the pyramidal layer showed a 14% decrease in cell number in mIFNγ injected mice compared to control mice; though no statistically significant change in cell diameter was evident (Suppl. Fig, 3L-N).

mIFNγ over-expression attenuates amyloid deposition in TgCRND8 mice

We next analyzed the effects of mIFNγ expression on Aβ deposition in the various expression paradigms. P2→5 month TgCRND8 mice expressing rAAV1-mIFNγ had significantly lower Aβ levels compared to rAAV1-EGFP expressing control mice as demonstrated by both immunohistological and biochemical analyses (Fig 2). There was a significant decrease in Aβ plaque burdens in the mIFNγ injected animals as shown by Aβ immunostaining (Fig 2 A-H). Quantification of Aβ plaque immunoreactivity in the forebrain and hippocampus of the P2→5 month mIFNγ injected TgCRND8 mice showed a 73% and 70% reduction in plaque burden, respectively (Fig 2, I-J). Biochemical analysis of Aβ levels in the SDS and FA solubilized mice brain lysates showed a similar magnitude of decrease in Aβ deposition following mIFNγ expression. In P2→5 month mIFNγ injected TgCRND8 mice, Aβ42 levels was decreased by 65% in the SDS and 79% in the FA fractions compared to control mice (Fig 2, K-L). Similarly, Aβ40 levels was decreased by 83% in the SDS and 85% in the FA fractions compared to control mice (Fig 2, K-L).

In the 4→5.5 month treatment paradigm, following immunohistochemical staining for Aβ, a 50% decrease in Aβ plaque burden was seen within the dissected coronal section in the mIFNγ expressing mice compared to EGFP injected mice (Fig 3, A-F, J). There was a 34% and 58% decrease in SDS extractable Aβ42 and Aβ40 levels respectively in mIFNγ expressing mice compared to controls (Fig 3, K). The FA fractions showed a 76% reduction in Aβ42 and a 47% reduction in Aβ40 levels in rAAV1-mIFNγ expressing mice compared to controls (Fig 3, L).

In an attempt to characterize whether the reduction in Aβ levels was due to active clearance of pre-deposited plaques or prevention of deposition, we analyzed the total Aβ plaque burden, Aβ42 as well as Aβ40 plaque burdens within the dissected coronal section of unmanipulated 4 month old TgCRND8 mice and 4→5.5 month experimental cohort (Fig 3; Suppl. Fig 4). Immunohistochemical analysis revealed that though the forebrain Aβ plaque burden in the 5.5 month old mIFNγ expressing mice is reduced compared to age matched controls, the total Aβ plaque burden of unmanipulated 4 month old mice is still lower than the mIFNγ expressing mice (Fig 3, G-J). To further probe whether there was a difference in the cored plaques (containing Aβ40) and diffuse plaques (containing Aβ42) in the 5.5 month old mIFNγ expressing mice compared to the age-matched controls and unmanipulated 4 month old controls, we quantified the forebrain plaque burden following immunostaining with Aβ40 (Suppl. Fig 4, A-C) and Aβ42 specific antibodies (Suppl. Fig 4, D-F). Our results show that there was a 45% decrease in Aβ42 plaque burden and a 32% decrease in Aβ40 plaque burden in the 5.5 month old mIFNγ expressing mice compared to age-matched EGFP expressing controls (Suppl. Fig 4, G). However, both the Aβ42 as well as Aβ40 burden of the unmanipulated 4 month old group remained lower than the mIFNγ expressing mice (Suppl. Fig 4, G).

Effect of mIFNγ on APP processing and Aβ production *in vivo*

To investigate whether mIFNγ induced reduction in Aβ levels in TgCRND8 mice is due to changes in APP processing or Aβ production, we conducted additional studies. We first measured APP levels in the RIPA extracted brains of mIFNγ over-expressing P2→5 month and 4→5.5 month TgCRND8 mice. We did not detect any significant changes in APP levels between control and mIFNγ over-expressing animals in P2→5 month cohorts (Fig 4, A-B). Nor were there any significant changes apparent in APP processing as measured by quantitation of APP C-terminal fragments (CTFα and CTFβ) in the P2→5 month mIFNγ injected group compared to controls (Fig 4, C-D). Similarly, in the 4→5.5 month mIFNγ injected adult TgCRND8 mice, no changes in APP levels or CTFα levels were seen (Fig 4, E-F).

To further probe whether mIFNγ influences the endogenous levels of APP or Aβ through cellular interaction with transcriptional or post-transcriptional mechanisms, we also analyzed the effects of rAAV1-mIFNγ expression in P2→5 month APP TgCRND8 non-transgenic littermates. We did not detect any change in endogenous APP levels (Suppl. Fig 5, A-B) or in steady state levels of endogenous Aβx-40 levels between the mIFNγ injected mice and control cohorts (Suppl. Fig 5, C). To investigate whether mIFNγ expression could alter the steady state Aβ levels in Tg2576 mice, neonatal Tg2576 pups were injected with rAAV1-mIFNγ or rAAV1-EGFP. Steady state APP and Aβ 40 levels were analyzed at 3 months of age, well before the onset of Aβ deposition, to avoid interference from possible contamination of deposited Aβ plaques in the ELISA measurements. In spite of significantly increased gliosis in the brains of mIFNγ expressing Tg2576 mice (data not shown), there was no statistically significant changes in APP and CTF levels (Suppl. Fig 5, D-E) or in steady state Aβ40 levels in rAAV1-mIFNγ expressing mice compared to the EGFP injected mice (Suppl. Fig 5, F). Thus, our present data show that, even in the presence of high levels of mIFNγ expression in the brain, there is no significant change in either APP processing or steady state Aβ production levels in APP transgenic and non-transgenic littermates *in vivo.*

Next we investigated whether the attenuation in Aβ levels is due to alterations in Aβ degrading enzymes, like Neprilysin or Insulin Degrading Enzyme (IDE). Q-PCR analysis showed no change in mRNA transcript levels in either of these enzymes in mIFNγ expressing mice compared to controls (Suppl. Fig 6, A). Since IFNγ has been reported to induce BACE expression by direct binding of STAT1 to BACE1 promoter in astrocytic cultures (35), we investigated whether increased glial activation in the mIFNγ expressing mice leads to alterations in BACE1 levels. We did not detect any significant change in BACE1 levels in P2→5 month old TgCRND8 mice injected with mIFNγ compared to control mice in spite of increased glial activation in these mice (Suppl. Fig 6, B-C).

mIFNγ expression enhances microglial phagocytosis *in vitro* and leads to upregulation of complement proteins *in vivo*

In the absence of detectable changes in steady state Aβ levels, APP expression and APP processing, we first explored whether the amelioration of Aβ deposition in mIFNγ expressing TgCRND8 mice could be due to enhanced phagocytosis of Aβ aggregates by activated microglia. Using *in vitro* culture experiments, we show that pretreatment of mouse primary microglia cells with recombinant mIFNγ upregulates the expression of CD68 (Scavenger Receptor class D), an endosomal/lysosomal marker associated with increased phagocytosis (Suppl. Fig 7, A-C). Using fluorescent tagged fibrillar Aβ42 aggregates (Hilyte 568-fAβ42), we also detected increased fAβ42 uptake by the mouse microglia cells that were primed with recombinant mIFNγ compared to untreated glia (Suppl. Fig 7, D-F).

To examine whether peripheral macrophages are involved in Aβ removal, we examined whether increased levels of CD45 is associated with Congophilic plaques in mIFNγ expressing mice (Suppl. Fig 8). However, we could not find any cored plaques in the P2→5 month experimental group that were immunopositive for CD45 (Suppl. Fig. 8, A-C). To further probe the involvement of peripheral immune cells in Aβ removal, we used Ly-6c, a marker for bone marrow derived inflammatory monocytes (36) in conjunction with Congo Red histological stain. We found that though Ly-6C+ monocytes are present in the parenchyma of the mIFNγ expressing mice brains, none are associated with Congophilic plaques in these mice (Suppl. Fig 8, D-F).

Next, we attempted to evaluate the expression status of multiple microglial markers *in vivo* by using real time Q-PCR of mRNA transcripts following P2→5mo rAAV1-mIFNγ expression in TgCRND8 mice forebrain. There were significant increases in MHCI, MHCII and CD11c transcript levels in mIFNγ expressing mice compared to controls (Fig 5, A). We

noticed modest increases in inducible NOS (iNOS), Scavenger Receptor Class A (SR-A) CD68 and CCR2 levels (Fig 5, A). However, analysis of two alternative "M2" microglial phenotype markers, Ym-1 and Arg (Arginase), that have been recently reported as potential markers for enhanced microglia-mediated Aβ phagocytosis (37, 38) showed that these were unchanged in mIFNγ expressing mice (Fig 5, A). We then performed Q-PCR analysis of murine cytokine mRNA transcript levels and observed significant increases in IFNγ and TNFα transcript levels (Fig 5, B). No significant changes were seen in the transcript levels of IL-1β, IL-6, IL-4, TGFβ and IL-10 (Fig 5, B).

We also analyzed both mRNA transcript levels and protein levels of components of the complement system as IFNγ has been previously shown to directly stimulate transcription or stabilize complement C3 and C4 mRNAs (39, 40). Q-PCR analysis revealed significant upregulation of complement C1q, C3, and C4a mRNA transcript levels in mIFNγ expressing mice compared to age-matched controls (Fig 6, A). Complement C5a and mouse complement receptor CR1/2 mRNA transcript levels were not altered (Fig 6, A). Next, we measured whether there was any increase in C3 protein levels itself. Immunoblotting analysis showed that protein levels of C3 were significantly increased in TgCRND8 expressing mIFNγ compared to age-matched controls (Fig 6, B-C). Immunofluorescence analysis also showed increased immunoreactivity of neuronally expressed complement protein C3 in mIFNγ expressing mice (Fig 6, D-I).

Discussion

Pro-inflammatory stimuli, including cytokines like IL1β, IL-6 and IFNγ, in the brain have been proposed to exacerbate the existing AD neuropathology (18, 41). In this study, we used two different *in vivo* experimental paradigms to investigate the role of mIFNγ on Aβ attenuation: the P2→5 month expression paradigm that examines largely non-neuronal expression of mIFNγ in the brain and the 4→5.5 month expression paradigm, that tests the neuronal expression of mIFNγ (in the hippocampus). In both of these experimental procedures, we observed comparable levels of glial activation and Aβ attenuation. The widespread presence of activated glia in both these paradigms indicates that non-cell autonomous effects of mIFNγ are likely responsible for the glial phenotype and Aβ suppression.

A proposed pathogenic role for IFNγ and other pro-inflammatory mediators in AD is largely rooted in previous reports showing that pro-inflammatory cytokines upregulate APP expression, APP processing and Aβ production leading to enhanced Aβ accumulation and self-perpetuation of Aβ aggregate-induced neurotoxicity (11, 13, 27, 41). Here we demonstrate that CNS expression of mIFNγ does not significantly alter APP processing as we did not observe any changes in APP levels in transgenic mice from both experimental paradigms. Importantly, we did not observe any change in the steady state Aβ production in young APP transgenic mice expressing mIFNγ. Notably, we did not observe any changes in endogenous APP or Aβ levels in APP non-transgenic mice, demonstrating that mIFNγ induced neuroinflammation in the brain does not transcriptionally alter the amyloidogenic pathway during the early phases of plaque deposition. In addition, we did not observe any changes in BACE enzyme or Aβ degrading enzymes (i.e., IDE and Neprilysin) in mIFNγ expressing TgCRND8 mice. Rather, our data shows that expression of mIFNγ results in significant Aβ attenuation in TgCRND8 mice, irrespective of whether mIFNγ expression is initiated prior to Aβ deposition or in adult mice with pre-existing Aβ deposits. In a recent study, 10 month expression of rAAV1-human IFNγ in the hippocampus of triple transgenic mice 3XTg resulted in increased microgliosis, unaltered astrocytosis, and decreased tau pathology (28). No alterations in APP was noted, supporting our observations that pro-inflammatory cytokines are not amyloidogenic; however, the authors noted increased

intracellular Aβ levels in human IFNγ expressing mice compared to controls. All in all, given the low levels of human IFNγ expression in this model and no reports of changes in Aβ plaque burden, it is tenuous to draw any parallels between our observations and this mouse model.

IFNγ is a complex pleitropic molecule interacting with multiple intracellular targets (20). Since the prominent feature of our experimental model is gliosis and upregulation of phagocytic markers, with no changes in APP processing or Aβ production, we decided to investigate whether IFNγ induced enhanced phagocytosis has a role in attenuating Aβ aggregates. Activated microglia have been previously reported to clear soluble Aβ as well as Aβ aggregates both *in vitro* and *in vivo* (42–46). Indeed, IFNγ by itself has been shown to potently activate monocytes and macrophages, resulting in enhanced pinocytosis and receptor-mediated phagocytosis (reviewed in (20)). We find that pretreatment of primary mouse microglia cells with recombinant mIFNγ *in vitro* results in increased expression of a phagocytic marker (CD68) and enhanced uptake of Aβ aggregates. Similarly, mIFNγ expression in mouse brains resulted in modest upregulation of CD68 and scavenger receptor (SR-A), suggesting that mIFNγ induced uptake of aggregated Aβ by activated microglia *in vivo* could be mediated by these pathways.

Considering the complexities in real time imaging techniques to monitor Aβ clearance in vivo (44), direct evidence irrevocably showing the mechanism of glial Aβ clearance is challenging. Multiple groups have observed Aβ colocalized within microglial endolysosomal compartments (43), providing indirect evidence supporting Aβ uptake by glia. However, whether this is mediated by active clearance of cored plaques or attenuation of deposition remains to be seen. Following mIFNγ expression in adult mice with pre-existing plaques, analysis of the cored and diffuse Aβ plaques shows that the decrease in mIFNγ induced Aβ plaque burden is mediated through attenuation or prevention of deposition, rather than an active clearance process of already deposited cored plaques. It is possible that mIFNγ stimulated innate immune mediators are able to efficiently remove soluble or oligomeric Aβ, without affecting the already deposited cored plaques. Interestingly, in a 4 week long study in which microglia were completely ablated, it was shown that absence of microglia does not affect amyloid plaque formation, maintenance or clearance (47). This raises the intriguing possibility that naïve microglia does not have the ability to remove Aβ, as has been previously reported from AD patient brains and transgenic mouse models (48). Our study, on the other hand, demonstrates the feasibility of activating microglia using innate immune mediators, i.e., IL-1β, IL-6 or M-CSF, that results in efficacious functional activation *in vivo* (14, 19, 49).

mIFNγ expression *in vivo* also resulted in significant upregulation of MHCI, MHCII, CD11b and CD11c markers, suggesting non cell autonomous morphological and phenotypic glial activation. This microglial phenotype is reminiscent of a dendritic-like cell presentation previously reported to have a beneficial role in Aβ clearance under different experimental conditions (29, 50). For example, It has been shown that IFNγ expression enhanced Aβ clearance by activating CD11b/CD68 positive microglia and possible interactions with Aβ reactive CD4+ T cells following Aβ vaccination in APP/IFNγ bigenic mice (29). Non-Aβ vaccination strategies using glatiramer acetate also reportedly clear Aβ deposits in APP transgenic mice by inducing Th1 T cell responses and and presentation of dendritic cell-like APC phenotype (50, 51). However, in our study, we could not demonstrate the presence of T cells (by CD3 immunoreactivity) in the forebrains of the IFNγ expressing mice, precluding the possibility of T cell and microglial dendritic cell involvement. Additionally, we examined whether there are any bone marrow derived peripheral inflammatory monocytes or macrophages in the brain. These are phenotypically defined respectively as being Ly-6C^{hi}CCR2+CX3CR1^{lo} monocytes and CD45^{hi} macrophages (36). We detected increased

CCR2 by Q-PCR and Ly-6C by immunohistochemistry in IFNγ expressing mice brains. However, we did not detect either Ly-6c or CD45 immunopositive peripheral immune cells in close proximity to cored plaques, suggesting that in this model system, peripheral macrophages or monocytes may not play a direct role in Aβ clearance, in contrast to recent reports from other groups (52, 53). Given that the decrease in Aβ reduction is mediated through attenuation, it is possible that the activated immune cells may play a more significant role in removing diffuse Aβ, rather than cored Aβ plaques. However, we cannot exclude the possibility of transient involvement of either T cells or peripheral macrophages in this model.

To further define the microglial phenotype observed in this paradigm, we analyzed a subset of macrophage phenotypic markers recently described to be associated with Aβ clearance (37, 38). These include the alternative “M2” macrophage markers Ym-1, Arg and FIZZ1. Neither Ym-1 nor Arg levels were changed; however, the classical “M1” phenotype markers, iNOS and TNFα, were upregulated following IFNγ expression *in vivo*. Thus, the mIFNγ activated microglia in our study resemble the classical “M1” phenotype as opposed to the alternative “M2” phenotype (37). Though the M2 microglial phenotype has been hypothesized to be associated with enhanced Aβ removal (37), our data suggest that M1 microglia may be equally proficient in restricting Aβ pathology. Indeed, the nature of the inflammatory initiator and the context, timing and strength of the response are likely to be critically important factors that determine the experimental outcome. Therefore, it is challenging to define a restricted subset of microglial markers as predictive of the “beneficial” microglial function. Nevertheless, in this study, we have provided several lines of evidence to support a direct beneficial role of microglial involvement with respect to suppression of Aβ deposition *in vivo* following expression of mIFNγ.

Several recent studies have explored the relationship between complement proteins and Aβ (reviewed in (54)). Inhibition of the C3 convertase using a soluble complement receptor sCrry resulted in increased Aβ accumulation, demonstrating a potential beneficial role of complement C3 in Aβ removal (55). Similarly, C3 deficient APP transgenic mice show accelerated Aβ deposition (56). Complement C1q in association with Aβ deposits has also been thought to have a protective function by enhancing clearance of cellular debris and protecting neurons against Aβ toxicity (57). In our study, complement system components (e.g. C1q and C3) were significantly upregulated in mIFNγ expressing APP mice as measured by Q-PCR, immunohistochemical and immunoblotting methods, suggesting the potential role of complement proteins in Aβ attenuation. Since complement opsonins (C1q, and C3b) interact with surface receptors to promote phagocytosis, it is possible that a synergistic interaction between activated glia and complement proteins may contribute to enhanced Aβ phagocytosis. Interestingly, a recent genome-wide association study also identified complement component (3b/4b) receptor 1 (CR1) as one of several new genes potentially associated with increased risk for late onset AD (58).

Previous studies in genotypically diverse mouse models have shown that IFNγ or IFNα expression leads to tissue calcification (59, 60). We also find that mIFNγ expression in P2→5 month old APP TgCRND8 mice leads to calcification in the basal ganglia and thalamus. Although CNS calcification could influence amyloid deposition, we observed robust suppression of Aβ deposition in the 4→5.5 month expression paradigm with no accompanying calcification. Moreover, in the age range investigated (under 5.5 months of age), Aβ plaques are primarily deposited in the hippocampus and frontal cortex of TgCRND8 transgenic mice whereas the calcification is restricted to the basal ganglia and thalamus. Thus in the adult hippocampal injection paradigm, we see removal of Aβ without calcification and in the neonatal paradigm, the Aβ removal and occurrence of calcified

deposits is spatially distinct. This suggests that basal ganglia calcification and Aβ attenuation are separate and unrelated events.

In summary, we find mIFNγ expression in brains of TgCRND8 mice resulted in i) striking glial activation and up regulation of microglial activation markers MHCII, CD11b and CD11c; ii) upregulation of select complement factors *in vivo*; iii) increased fAβ phagocytosis by mIFNγ primed mouse microglia *in vitro*; iv) robust suppression of Aβ deposition *in vivo;* v) no evidence for alterations in APP processing or steady state Aβ levels. Our current results along with other recently published studies, suggest that activated microglia and complement proteins can significantly restrict Aβ deposition early in the disease process. However, the fact that Aβ aggregates continue to accumulate in the brain with age indicates that the resulting immune response to Aβ aggregates is clearly ineffective. This ineffective clearance may then result in a basal level of chronic immune activation that may contribute to AD type neurodegeneration (18). Although it may be feasible to transiently and selectively activate microglia to modify Aβ deposition in a manner that is both effective and tolerable, any intervention for AD based on activation of the innate immune system clearly must strike a balance between neuroprotective and neurotoxic effects.

Supplementary Material

Refer to Web version on PubMed Central for supplementary material.

Acknowledgments

The authors would like to thank Monica Castanedes-Casey, Virginia Phillips and Linda Rousseau for assistance with tissue processing and immunohistochemical analyses; Faith Conkle, Deborah Maloy and the Mayo Clinic Veterinary Medicine staff for animal maintenance.

Grant Support: This work was supported by Mayo Clinic (TEG), National Institutes of Health/National Institute on Aging Grants (RO1AG18454, RO1AG29886, P01AG25531; TEG), American Health Assistance Foundation Grant A2009061 (PD) and a Robert H. and Clarice Smith Foundation post-doctoral fellowship (PC).

References

1. Wyss-Coray T. Inflammation in Alzheimer disease: driving force, bystander or beneficial response? Nat Med. 2006; 12:1005–1015. [PubMed: 16960575]
2. Vehmas AK, Kawas CH, Stewart WF, Troncoso JC. Immune reactive cells in senile plaques and cognitive decline in Alzheimer's disease. Neurobiol Aging. 2003; 24:321–331. [PubMed: 12498966]
3. Cagnin A, Brooks DJ, Kennedy AM, Gunn RN, Myers R, Turkheimer FE, Jones T, Banati RB. In-vivo measurement of activated microglia in dementia. Lancet. 2001; 358:461–467. [PubMed: 11513911]
4. Yan SD, Chen X, Fu J, Chen M, Zhu H, Roher A, Slattery T, Zhao L, Nagashima M, Morser J, Migheli A, Nawroth P, Stern D, Schmidt AM. RAGE and amyloid-beta peptide neurotoxicity in Alzheimer's disease. Nature. 1996; 382:685–691. [PubMed: 8751438]
5. El Khoury J, Hickman SE, Thomas CA, Cao L, Silverstein SC, Loike JD. Scavenger receptor-mediated adhesion of microglia to betaamyloid fibrils. Nature. 1996; 382:716–719. [PubMed: 8751442]
6. Paresce DM, Ghosh RN, Maxfield FR. Microglial cells internalize aggregates of the Alzheimer's disease amyloid beta-protein via a scavenger receptor. Neuron. 1996; 17:553–565. [PubMed: 8816718]
7. Fassbender K, Walter S, Kuhl S, Landmann R, Ishii K, Bertsch T, Stalder AK, Muehlhauser F, Liu Y, Ulmer AJ, Rivest S, Lentschat A, Gulbins E, Jucker M, Staufenbiel M, Brechtel K, Walter J,

Multhaup G, Penke B, Adachi Y, Hartmann T, Beyreuther K. The LPS receptor (CD14) links innate immunity with Alzheimer's disease. Faseb J. 2004; 18:203–205. [PubMed: 14597556]

8. Tan J, Town T, Crawford F, Mori T, DelleDonne A, Crescentini R, Obregon D, Flavell RA, Mullan MJ. Role of CD40 ligand in amyloidosis in transgenic Alzheimer's mice. Nat Neurosci. 2002; 5:1288–1293. [PubMed: 12402041]
9. Leuner K, Hauptmann S, Abdel-Kader R, Scherping I, Keil U, Strosznajder JB, Eckert A, Muller WE. Mitochondrial dysfunction: the first domino in brain aging and Alzheimer's disease? Antioxid Redox Signal. 2007; 9:1659–1675. [PubMed: 17867931]
10. Butterfield DA, Reed T, Newman SF, Sultana R. Roles of amyloid beta-peptide-associated oxidative stress and brain protein modifications in the pathogenesis of Alzheimer's disease and mild cognitive impairment. Free Radic Biol Med. 2007; 43:658–677. [PubMed: 17664130]
11. Liao YF, Wang BJ, Cheng HT, Kuo LH, Wolfe MS. Tumor necrosis factor-alpha, interleukin-1beta, and interferon-gamma stimulate gamma-secretase-mediated cleavage of amyloid precursor protein through a JNK-dependent MAPK pathway. J Biol Chem. 2004; 279:49523–49532. [PubMed: 15347683]
12. Heneka MT, Sastre M, Dumitrescu-Ozimek L, Dewachter I, Walter J, Klockgether T, Van Leuven F. Focal glial activation coincides with increased BACE1 activation and precedes amyloid plaque deposition in APP[V717I] transgenic mice. J Neuroinflammation. 2005; 2:22. [PubMed: 16212664]
13. Yamamoto M, Kiyota T, Horiba M, Buescher JL, Walsh SM, Gendelman HE, Ikezu T. Interferon-gamma and tumor necrosis factoralpha regulate amyloid-beta plaque deposition and beta-secretase expression in Swedish mutant APP transgenic mice. Am J Pathol. 2007; 170:680–692. [PubMed: 17255335]
14. Shaftel SS, Kyrkanides S, Olschowka JA, Miller JN, Johnson RE, O'Banion MK. Sustained hippocampal IL-1 beta overexpression mediates chronic neuroinflammation and ameliorates Alzheimer plaque pathology. J Clin Invest. 2007; 117:1595–1604. [PubMed: 17549256]
15. Scholtzova H, Kascsak RJ, Bates KA, Boutajangout A, Kerr DJ, Meeker HC, Mehta PD, Spinner DS, Wisniewski T. Induction of tolllike receptor 9 signaling as a method for ameliorating Alzheimer's disease-related pathology. J Neurosci. 2009; 29:1846–1854. [PubMed: 19211891]
16. Tahara K, Kim HD, Jin JJ, Maxwell JA, Li L, Fukuchi K. Role of toll-like receptor signalling in Abeta uptake and clearance. Brain. 2006; 129:3006–3019. [PubMed: 16984903]
17. Richard KL, Filali M, Prefontaine P, Rivest S. Toll-like receptor 2 acts as a natural innate immune receptor to clear amyloid beta 1–42 and delay the cognitive decline in a mouse model of Alzheimer's disease. J Neurosci. 2008; 28:5784–5793. [PubMed: 18509040]
18. Wyss-Coray T, Mucke L. Inflammation in neurodegenerative disease--a double-edged sword. Neuron. 2002; 35:419–432. [PubMed: 12165466]
19. Chakrabarty P, Jansen-West K, Beccard A, Ceballos-Diaz C, Levites Y, Verbeeck C, Zubair AC, Dickson D, Golde TE, Das P. Massive gliosis induced by interleukin-6 suppresses A{beta} deposition in vivo: evidence against inflammation as a driving force for amyloid deposition. Faseb J. 2009
20. Schroder K, Hertzog PJ, Ravasi T, Hume DA. Interferongamma: an overview of signals, mechanisms and functions. J Leukoc Biol. 2004; 75:163–189. [PubMed: 14525967]
21. Neumann H, Boucraut J, Hahnel C, Misgeld T, Wekerle H. Neuronal control of MHC class II inducibility in rat astrocytes and microglia. Eur J Neurosci. 1996; 8:2582–2590. [PubMed: 8996807]
22. Colangelo V, Schurr J, Ball MJ, Pelaez RP, Bazan NG, Lukiw WJ. Gene expression profiling of 12633 genes in Alzheimer hippocampal CA1: transcription and neurotrophic factor down-regulation and upregulation of apoptotic and pro-inflammatory signaling. J Neurosci Res. 2002; 70:462–473. [PubMed: 12391607]
23. Ricciarelli R, d'Abramo C, Massone S, Marinari U, Pronzato M, Tabaton M. Microarray analysis in Alzheimer's disease and normal aging. IUBMB Life. 2004; 56:349–354. [PubMed: 15370883]
24. Abbas N, Bednar I, Mix E, Marie S, Paterson D, Ljungberg A, Morris C, Winblad B, Nordberg A, Zhu J. Up-regulation of the inflammatory cytokines IFN-gamma and IL-12 and down-regulation

of IL-4 in cerebral cortex regions of APP(SWE) transgenic mice. J Neuroimmunol. 2002; 126:50–57. [PubMed: 12020956]

25. Apelt J, Schliebs R. Beta-amyloid-induced glial expression of both pro- and anti-inflammatory cytokines in cerebral cortex of aged transgenic Tg2576 mice with Alzheimer plaque pathology. Brain Res. 2001; 894:21–30. [PubMed: 11245811]
26. Patel NS, Paris D, Mathura V, Quadros AN, Crawford FC, Mullan MJ. Inflammatory cytokine levels correlate with amyloid load in transgenic mouse models of Alzheimer's disease. J Neuroinflammation. 2005; 2:9. [PubMed: 15762998]
27. Blasko I, Marx F, Steiner E, Hartmann T, Grubeck-Loebenstein B. TNFalpha plus IFNgamma induce the production of Alzheimer betaamyloid peptides and decrease the secretion of APPs. Faseb J. 1999; 13:63–68. [PubMed: 9872930]
28. Mastrangelo MA, Sudol KL, Narrow WC, Bowers WJ. Interferon-{gamma} differentially affects Alzheimer's disease pathologies and induces neurogenesis in triple transgenic-AD mice. Am J Pathol. 2009; 175:2076–2088. [PubMed: 19808651]
29. Monsonego A, Imitola J, Petrovic S, Zota V, Nemirovsky A, Baron R, Fisher Y, Owens T, Weiner HL. Abeta-induced meningoencephalitis is IFN-gamma-dependent and is associated with T celldependent clearance of Abeta in a mouse model of Alzheimer's disease. Proc Natl Acad Sci U S A. 2006; 103:5048–5053. [PubMed: 16549802]
30. Baron R, Nemirovsky A, Harpaz I, Cohen H, Owens T, Monsonego A. IFN-gamma enhances neurogenesis in wild-type mice and in a mouse model of Alzheimer's disease. Faseb J. 2008; 22:2843–2852. [PubMed: 18390924]
31. Chishti MA, Yang DS, Janus C, Phinney AL, Horne P, Pearson J, Strome R, Zuker N, Loukides J, French J, Turner S, Lozza G, Grilli M, Kunicki S, Morissette C, Paquette J, Gervais F, Bergeron C, Fraser PE, Carlson GA, George-Hyslop PS, Westaway D. Early-onset amyloid deposition and cognitive deficits in transgenic mice expressing a double mutant form of amyloid precursor protein 695. J Biol Chem. 2001; 276:21562–21570. [PubMed: 11279122]
32. Hsiao K, Chapman P, Nilsen S, Eckman C, Harigaya Y, Younkin S, Yang F, Cole G. Correlative memory deficits, Abeta elevation, and amyloid plaques in transgenic mice [see comments]. Science. 1996; 274:99–102. [PubMed: 8810256]
33. Kim J, Miller VM, Levites Y, West KJ, Zwizinski CW, Moore BD, Troendle FJ, Bann M, Verbeeck C, Price RW, Smithson L, Sonoda L, Wagg K, Rangachari V, Zou F, Younkin SG, Graff-Radford N, Dickson D, Rosenberry T, Golde TE. BRI2 (ITM2b) inhibits Abeta deposition in vivo. J Neurosci. 2008; 28:6030–6036. [PubMed: 18524908]
34. Howard V, Reid S, Baddeley A, Boyde A. Unbiased estimation of particle density in the tandem scanning reflected light microscope. J Microsc. 1985; 138:203–212. [PubMed: 4020859]
35. Cho HJ, Kim SK, Jin SM, Hwang EM, Kim YS, Huh K, Mook-Jung I. IFN-gamma-induced BACE1 expression is mediated by activation of JAK2 and ERK1/2 signaling pathways and direct binding of STAT1 to BACE1 promoter in astrocytes. Glia. 2007; 55:253–262. [PubMed: 17091494]
36. Davoust N, Vuaillat C, Androdias G, Nataf S. From bone marrow to microglia: barriers and avenues. Trends Immunol. 2008; 29:227–234. [PubMed: 18396103]
37. Jimenez S, Baglietto-Vargas D, Caballero C, Moreno-Gonzalez I, Torres M, Sanchez-Varo R, Ruano D, Vizuete M, Gutierrez A, Vitorica J. Inflammatory response in the hippocampus of PS1M146L/APP751SL mouse model of Alzheimer's disease: age-dependent switch in the microglial phenotype from alternative to classic. J Neurosci. 2008; 28:11650–11661. [PubMed: 18987201]
38. Morgan D, Gordon MN, Tan J, Wilcock D, Rojiani AM. Dynamic complexity of the microglial activation response in transgenic models of amyloid deposition: implications for Alzheimer therapeutics. J Neuropathol Exp Neurol. 2005; 64:743–753. [PubMed: 16141783]
39. Barnum SR, Jones JL, Benveniste EN. Interferon-gamma regulation of C3 gene expression in human astroglioma cells. J Neuroimmunol. 1992; 38:275–282. [PubMed: 1601980]
40. Mitchell TJ, Naughton M, Norsworthy P, Davies KA, Walport MJ, Morley BJ. IFN-gamma up-regulates expression of the complement components C3 and C4 by stabilization of mRNA. J Immunol. 1996; 156:4429–4434. [PubMed: 8666817]

41. Griffin WS, Sheng JG, Royston MC, Gentleman SM, McKenzie JE, Graham DI, Roberts GW, Mrak RE. Glial-neuronal interactions in Alzheimer's disease: the potential role of a 'cytokine cycle' in disease progression. Brain Pathol. 1998; 8:65–72. [PubMed: 9458167]
42. Schenk D, Barbour R, Dunn W, Gordon G, Grajeda H, Guido T, Hu K, Huang J, Johnson-Wood K, Khan K, Kholodenko D, Lee M, Liao Z, Lieberburg I, Motter R, Mutter L, Soriano F, Shopp G, Vasquez N, Vandevert C, Walker S, Wogulis M, Yednock T, Games D, Seubert P. Immunization with amyloid-beta attenuates Alzheimer-disease-like pathology in the PDAPP mouse [see comments]. Nature. 1999; 400:173–177. [PubMed: 10408445]
43. Bolmont T, Haiss F, Eicke D, Radde R, Mathis CA, Klunk WE, Kohsaka S, Jucker M, Calhoun ME. Dynamics of the microglial/amyloid interaction indicate a role in plaque maintenance. J Neurosci. 2008; 28:4283–4292. [PubMed: 18417708]
44. Bacskai BJ, Kajdasz ST, Christie RH, Carter C, Games D, Seubert P, Schenk D, Hyman BT. Imaging of amyloid-beta deposits in brains of living mice permits direct observation of clearance of plaques with immunotherapy. Nat Med. 2001; 7:369–372. [PubMed: 11231639]
45. El Khoury J, Toft M, Hickman SE, Means TK, Terada K, Geula C, Luster AD. Ccr2 deficiency impairs microglial accumulation and accelerates progression of Alzheimer-like disease. Nat Med. 2007; 13:432–438. [PubMed: 17351623]
46. Mandrekar S, Jiang Q, Lee CY, Koenigsknecht-Talboo J, Holtzman DM, Landreth GE. Microglia mediate the clearance of soluble Abeta through fluid phase macropinocytosis. J Neurosci. 2009; 29:4252–4262. [PubMed: 19339619]
47. Grathwohl SA, Kalin RE, Bolmont T, Prokop S, Winkelmann G, Kaeser SA, Odenthal J, Radde R, Eldh T, Gandy S, Aguzzi A, Staufenbiel M, Mathews PM, Wolburg H, Heppner FL, Jucker M. Formation and maintenance of Alzheimer's disease beta-amyloid plaques in the absence of microglia. Nat Neurosci. 2009; 12:1361–1363. [PubMed: 19838177]
48. Jucker M, Heppner FL. Cerebral and peripheral amyloid phagocytes--an old liaison with a new twist. Neuron. 2008; 59:8–10. [PubMed: 18614025]
49. Boissonneault V, Filali M, Lessard M, Relton J, Wong G, Rivest S. Powerful beneficial effects of macrophage colony-stimulating factor on beta-amyloid deposition and cognitive impairment in Alzheimer's disease. Brain. 2009; 132:1078–1092. [PubMed: 19151372]
50. Butovsky O, Koronyo-Hamaoui M, Kunis G, Ophir E, Landa G, Cohen H, Schwartz M. Glatiramer acetate fights against Alzheimer's disease by inducing dendritic-like microglia expressing insulin-like growth factor-1. Proc Natl Acad Sci U S A. 2006; 103:11784–11789. [PubMed: 16864778]
51. Frenkel D, Maron R, Burt DS, Weiner HL. Nasal vaccination with a proteosome-based adjuvant and glatiramer acetate clears beta-amyloid in a mouse model of Alzheimer disease. J Clin Invest. 2005; 115:2423–2433. [PubMed: 16100572]
52. Simard AR, Rivest S. Bone marrow stem cells have the ability to populate the entire central nervous system into fully differentiated parenchymal microglia. Faseb J. 2004; 18:998–1000. [PubMed: 15084516]
53. Town T, Laouar Y, Pittenger C, Mori T, Szekely CA, Tan J, Duman RS, Flavell RA. Blocking TGF-beta-Smad2/3 innate immune signaling mitigates Alzheimer-like pathology. Nat Med. 2008; 14:681–687. [PubMed: 18516051]
54. Tenner AJ. Complement in Alzheimer's disease: opportunities for modulating protective and pathogenic events. Neurobiol Aging. 2001; 22:849–861. [PubMed: 11754992]
55. Wyss-Coray T, Yan F, Lin AH, Lambris JD, Alexander JJ, Quigg RJ, Masliah E. Prominent neurodegeneration and increased plaque formation in complement-inhibited Alzheimer's mice. Proc Natl Acad Sci U S A. 2002; 99:10837–10842. [PubMed: 12119423]
56. Maier M, Peng Y, Jiang L, Seabrook TJ, Carroll MC, Lemere CA. Complement C3 deficiency leads to accelerated amyloid beta plaque deposition and neurodegeneration and modulation of the microglia/macrophage phenotype in amyloid precursor protein transgenic mice. J Neurosci. 2008; 28:6333–6341. [PubMed: 18562603]
57. Pisalyaput K, Tenner AJ. Complement component C1q inhibits beta-amyloid- and serum amyloid P-induced neurotoxicity via caspaseand calpain-independent mechanisms. J Neurochem. 2008; 104:696–707. [PubMed: 17986223]

58. Lambert JC, Heath S, Even G, Campion D, Sleegers K, Hiltunen M, Combarros O, Zelenika D, Bullido MJ, Tavernier B, Letenneur L, Bettens K, Berr C, Pasquier F, Fievet N, Barberger-Gateau P, Engelborghs S, De Deyn P, Mateo I, Franck A, Helisalmi S, Porcellini E, Hanon O, de Pancorbo MM, Lendon C, Dufouil C, Jaillard C, Leveillard T, Alvarez V, Bosco P, Mancuso M, Panza F, Nacmias B, Bossu P, Piccardi P, Annoni G, Seripa D, Galimberti D, Hannequin D, Licastro F, Soininen H, Ritchie K, Blanche H, Dartigues JF, Tzourio C, Gut I, Van Broeckhoven C, Alperovitch A, Lathrop M, Amouyel P. Genome-wide association study identifies variants at CLU and CR1 associated with Alzheimer's disease. Nat Genet. 2009; 41:1094–1099. [PubMed: 19734903]

59. Shelton GD, Calcutt NA, Garrett RS, Gu D, Sarvetnick N, Campana WM, Powell HC. Necrotizing myopathy induced by overexpression of interferon-gamma in transgenic mice. Muscle Nerve. 1999; 22:156–165. [PubMed: 10024128]

60. Wang J, Schreiber RD, Campbell IL. STAT1 deficiency unexpectedly and markedly exacerbates the pathophysiological actions of IFNalpha in the central nervous system. Proc Natl Acad Sci U S A. 2002; 99:16209–16214. [PubMed: 12461178]

Abbreviations

P2→5 month old	Mice pups injected on day P2 and euthanized at 5 months
4→5.5 month old	Adult mice injected in the hippocampus at 4 month and euthanized at 5.5 months
AD	Alzheimer’s Disease
Aβ	Amyloid β
APP	Amyloid β Precursor Protein
Arg	Arginase
BACE	β-site APP-Cleaving Enzyme
CTF	C-terminal fragment
CNS	Central Nervous System
CR	Complement Receptor
EGFP	Enhanced Green Fluorescent Protein
fAβ	Fibrillar Aβ
FA	Formic Acid
GFAP	Glial Fibrillary Acidic Protein
Iba-1	Ionized calcium-binding adaptor molecule 1
iNOS	inducible Nitrogen Oxide synthase
mIFNγ	murine IFNγ
non-Tg	non-transgenic
Q-PCR	Real time Quantitative PCR on reverse transcribed mRNA
rAAV1	recombinant adeno associated virus serotype 1
SR-A	Scavenger Receptor A
Tg	Transgenic

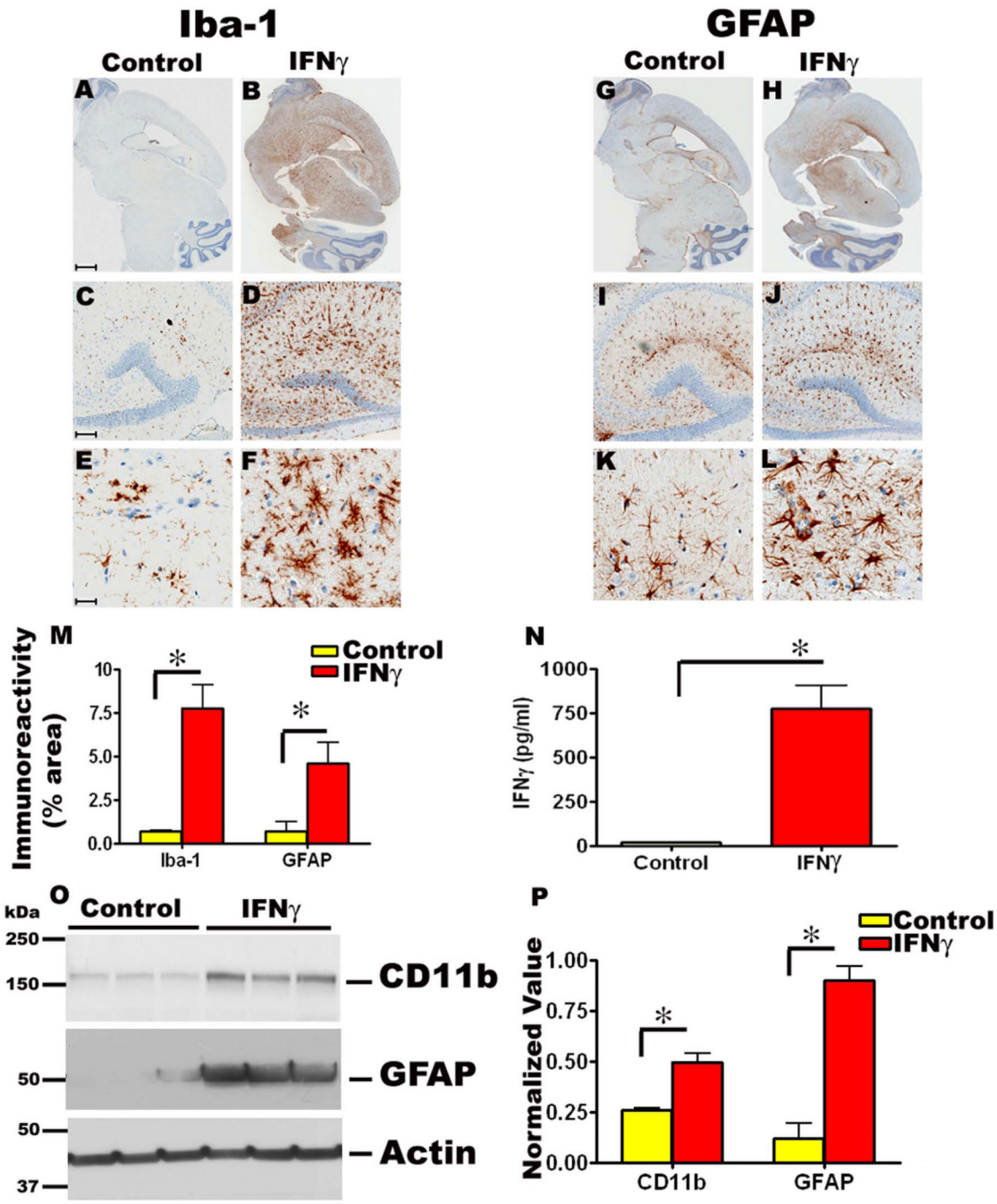

Fig 1. rAAV1-mIFNγ expression in TgCRND8 mice following neonatal intracerebroventricular injection results in extensive induction of microgliosis and astrogliosis

A-F. rAAV1-mIFNγ or rAAV1-EGFP (Control mice) was injected into the cerebral ventricles of TgCRND8 mice on neonatal day P2 and sacrificed after 5 months (P2→5mo). Representative images of Iba-1 immunoreactivity in paraffin embedded whole brain sections (A, B) and higher magnifications of the hippocampus (lower panels, C-F) is shown. Abundant activated microglia displaying hypertrophic processes are present in mIFNγ expressing mice (B, D, F) compared to EGFP expressing control mice (A, C, E). *Scale Bar,* 600μm (A, B), 150μm (C, D) and 25μm (E, F). *n*=10/group.

G-L. Representative images of GFAP immunoreactivity in paraffin embedded sections of P2→5 month old TgCRND8 mice expressing mIFNγ or EGFP is depicted. Whole brain sections (G, H) along with higher magnification pictures (lower panels, I-L) showing detailed morphology of the activated astrocytes in and around the corresponding hippocampus are shown. Abundant astrocytes are evident in mIFNγ expressing mice (H, J, L) compared to EGFP expressing control mice (G, I, K). *Scale Bar,* 600μm (G, H), 150μm (I, J) and 25μm (K, L). n=10/group.

M. Quantitation of Iba-1 and GFAP immunoreactivity burden (% area) in paraffin embedded sections of P2→5 month old TgCRND8 mice expressing mIFNγ or EGFP as control. (n=5/group, *p<0.05).

N. Levels of mIFNγ were increased in mIFNγ expressing P2→5 month old TgCRND8 mice brains compared to age-matched controls. mIFNγ protein levels were analyzed using RIPA buffer solubilized brain lysates by sandwich ELISA. (n=5/group, *p<0.05).

O-P. Representative immunoblot showing increased levels of CD11b and GFAP levels in P2→5 month old mIFNγ expressing TgCRND8 mice compared to controls (O). β-Actin has been used as a loading control. Intensity analysis of CD11b and GFAP immunoreactive bands normalized to β actin is depicted (P). (n=3/group, *p<0.05).

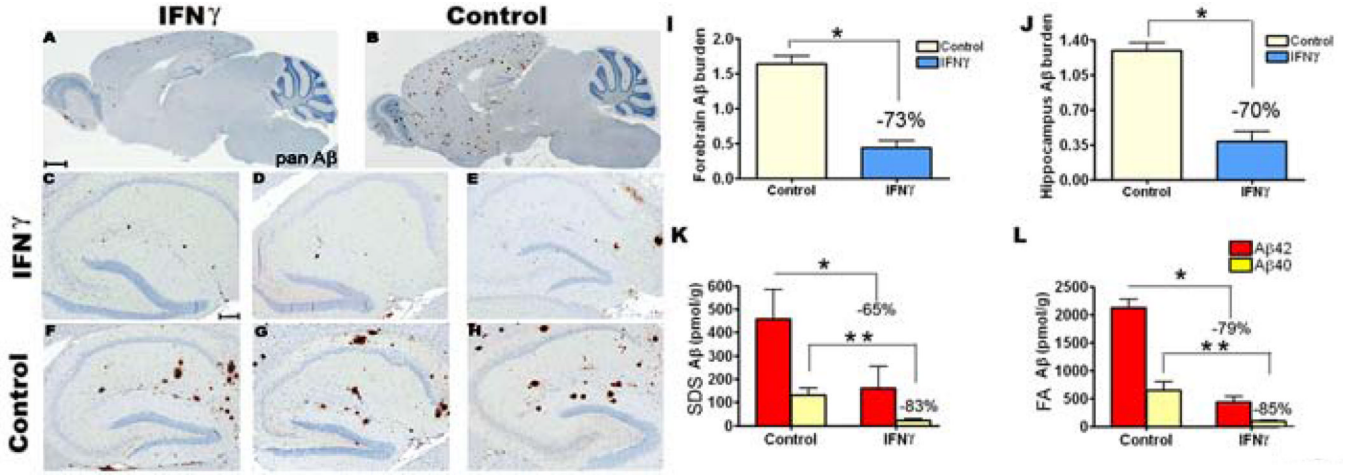

Fig 2. Significant attenuation of amyloid deposition in mIFNγ expressing (P2→5mo) TgCRND8 mice

A-H. rAAV1-mIFNγ or rAAV1-EGFP was injected into the cerebral ventricles of TgCRND8 mice on neonatal day P2 and sacrificed after 5 months (P2→5mo). mIFNγ expressing TgCRND8 mice (A, C-E) were analyzed along with age-matched EGFP expressing mice (B, F-H, Control). Representative sections of the whole brain (A-B) as well as hippocampus (C-H) from 3 mice from each group is shown following pan Aβ immunostaining. *Scale Bar,* 600μm (A-B), 150μm (C-H). n=10–12/group).

I-J. Image analysis of amyloid plaque immunoreactivity shows a significant decrease in Aβ plaque burdens in the forebrain (I) and hippocampus (J) of mIFNγ expressing mice compared to EGFP expressing control mice (n=10–12/group, *p<0.05).

K-L. Biochemical analyses of Aβ42 and Aβ40 levels in P2→5 month old mIFNγ expressing TgCRND8 mice compared to EGFP expressing age matched controls. Both SDS-soluble and SDS-insoluble (FA fraction) Aβ42 and Aβ40 levels in the forebrain of mIFNγ injected mice were significantly reduced compared to control mice (n=10/group, *p<0.05 and **p<0.05).

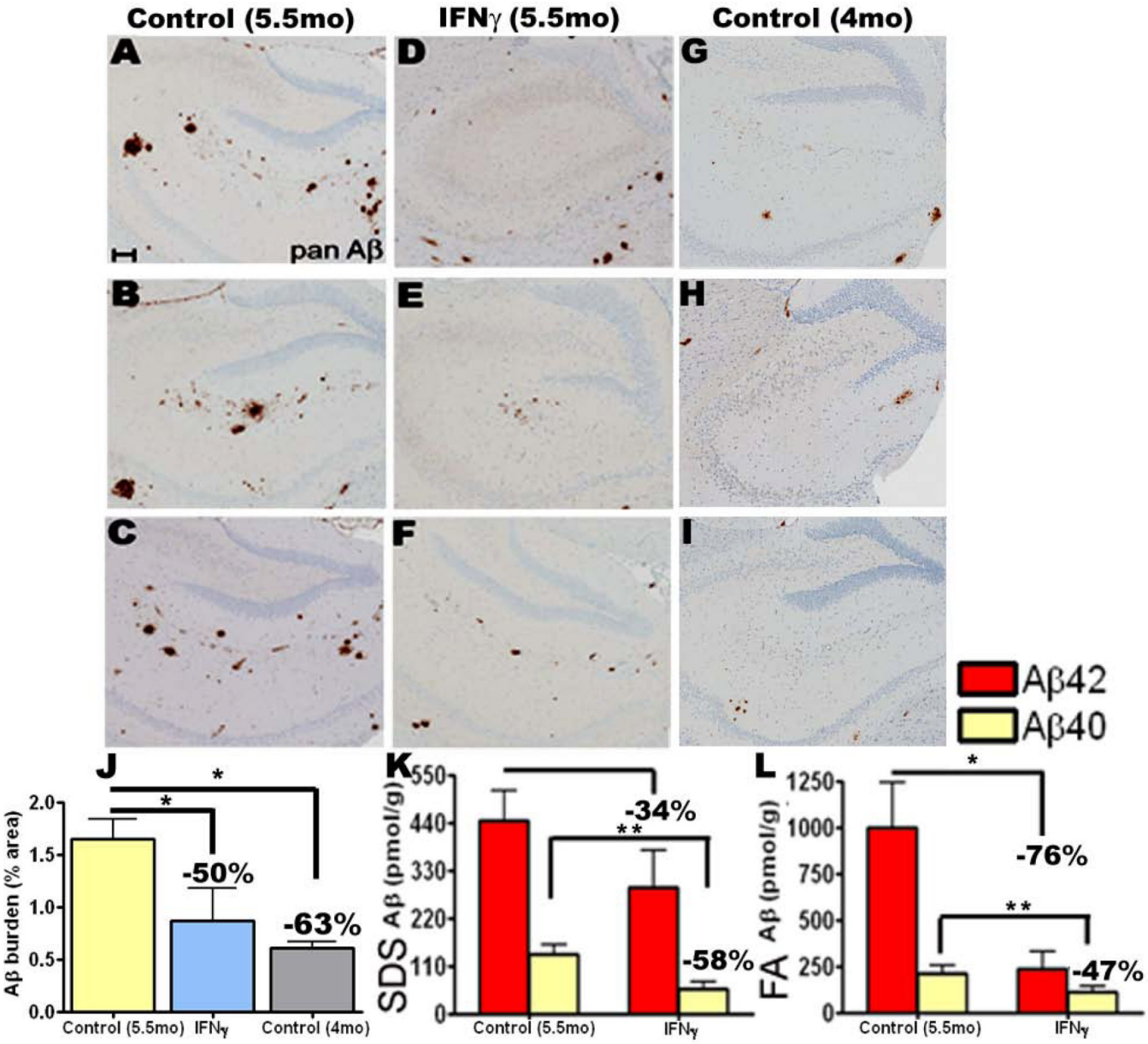

Fig 3. Amyloid deposition is suppressed following acute focal expression of mIFNγ in the hippocampus of TgCRND8 mice

A-I. 4 month old TgCRND8 mice were stereotaxically injected in the hippocampus with either rAAV1-mIFNγ or rAAV1-EGFP and sacrificed after 6 weeks. Representative brain sections stained with pan Aβ antibody depict attenuation of Aβ deposition in mIFNγ expressing mice (D-F) compared to EGFP injected controls (A-C) in the immediate vicinity of the injection site. Unmanipulated 4 month old TgCRND8 brains, dissected at the same level, are depicted (G-I). *Scale Bar*, 150μm. n=5/group.

J. Aβ plaque burden analysis shows a significant decrease in amyloid deposition in 5.5 month old mIFNγ expressing mice compared to EGFP expressing age-matched control mice but no change compared to unmanipulated 4 month old TgCRND8. (n=5/group, *p<0.05).

K-L. Biochemical analyses of Aβ42 and Aβ40 levels by ELISA show significant reductions in both SDS-soluble (H) and SDS-insoluble FA fractions (I) in mIFNγ expressing mice compared to controls (n=5/group, *p<0.05 and **p<0.05).

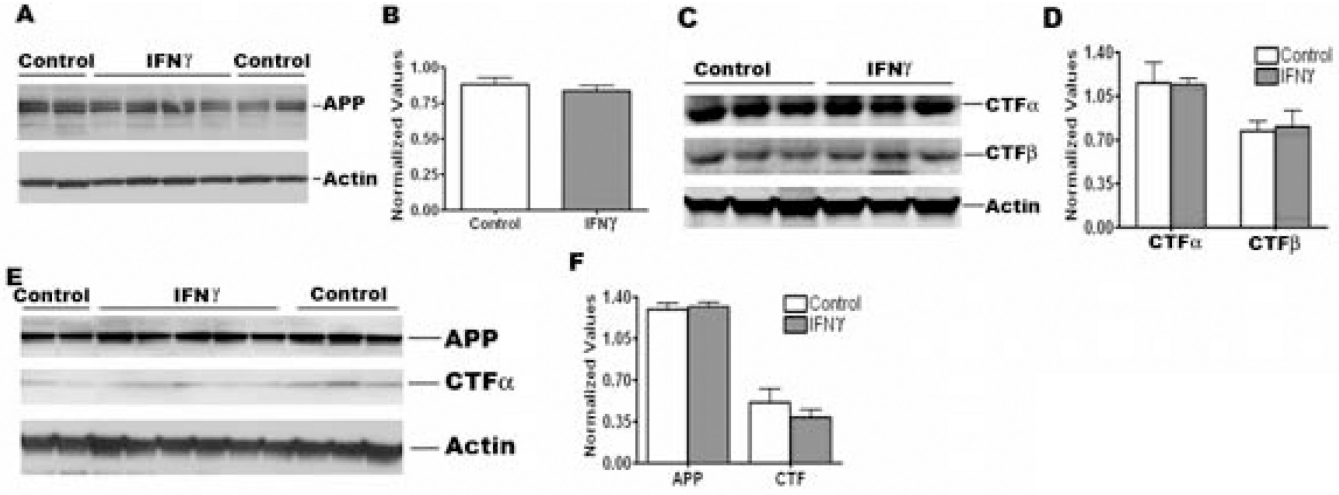

Fig 4. APP processing is not significantly altered in mIFNγ expressing P2→5 month old TgCRND8 mice

A-B. Representative anti CT20 immunoblot depicting APP levels in mIFNγ expressing P2→5 month old TgCRND8 and age-matched control mice (A). Intensity analysis of anti CT20 immunoreactive APP bands normalized to β-actin reveal no significant changes in APP levels in mIFNγ expressing TgCRND8 mice compared to age-matched controls (B). *n*=4/group.

C-D. Representative immunoblot showing CTFα (anti-CT20) and CTFβ (anti-82E1) levels in P2→5 month old TgCRND8 mice expressing mIFNγ or EGFP (C). Intensity analysis of CTFα and CTFβ bands normalized to β-actin reveal no significant changes in P2→5 month old TgCRND8 mice expressing mIFNγ compared to age-matched controls (D). *n*=3/group.

E-F. Representative anti CT20 immunoblot showing APP or CTFα levels in mIFNγ expressing 4→5.5 month old TgCRND8 mice and age-matched controls (E). Intensity analysis of APP and CTFα levels normalized to β-actin show no significant changes in 4→5.5 month old TgCRND8 mice expressing mIFNγ compared to age-matched controls (F). *n*=5/group.

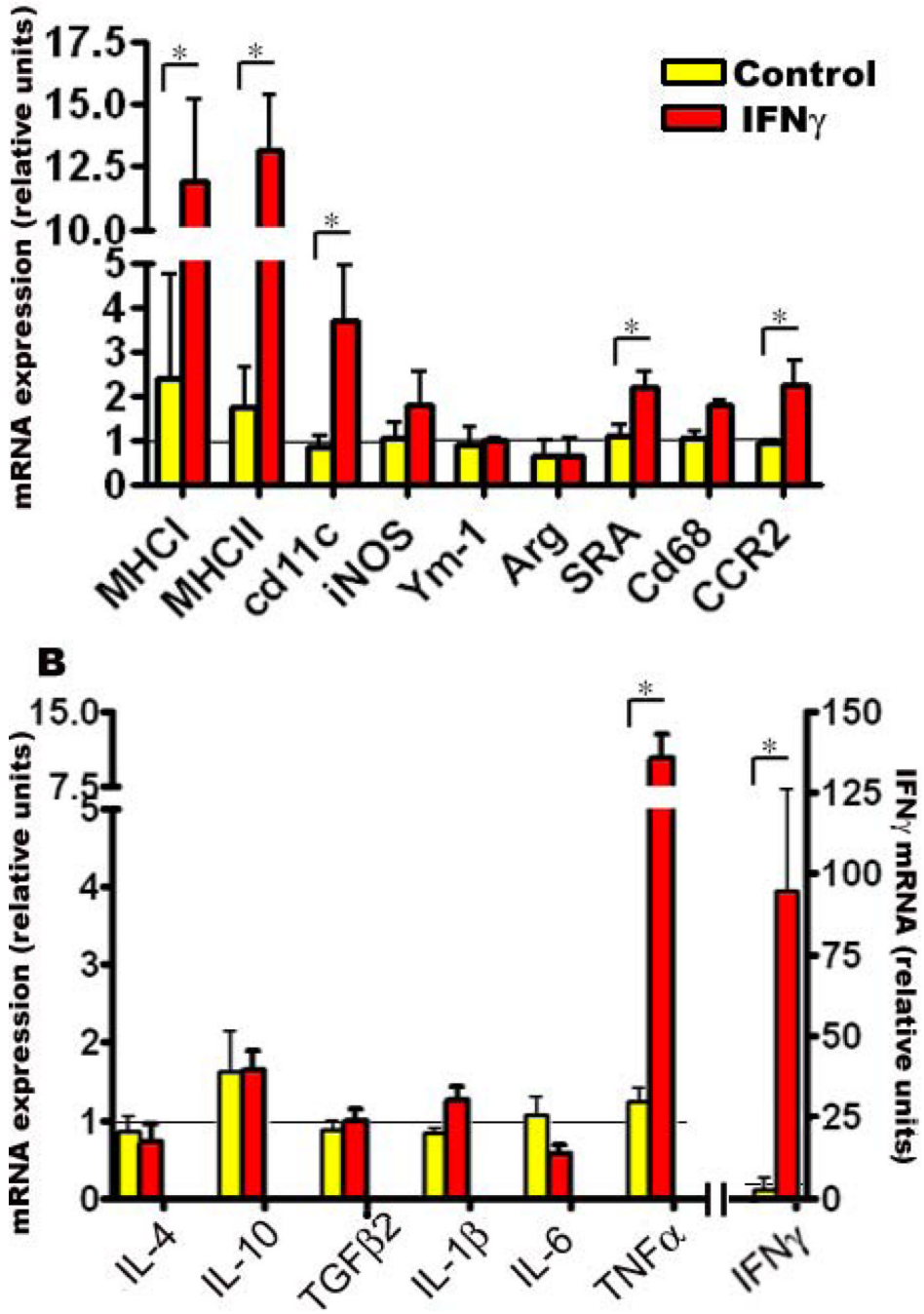

Fig 5. mIFNγ expression leads to alterations in glial activation markers and pro-inflammatory cytokines

Expression of glial activation markers (A) and cytokines (B) were determined in P2→5 month old mIFNγ expressing TgCRND8 mice compared to EGFP expressing age-matched transgenic controls using real time Q-PCR. Relative quantitation of mRNA transcript levels was performed using the comparative cycle threshold method. The expression levels of different genes were normalized using β-actin levels from the corresponding samples. Data, expressed as relative units of mRNA expression, represents averaged fold change values obtained from mIFNγ expressing mice, relative to averaged values obtained from EGFP

expressing mice. The horizontal line represents the reference point used for relative mRNA analysis. Error bars indicate SEM. (n=4/group, *p<0.05).

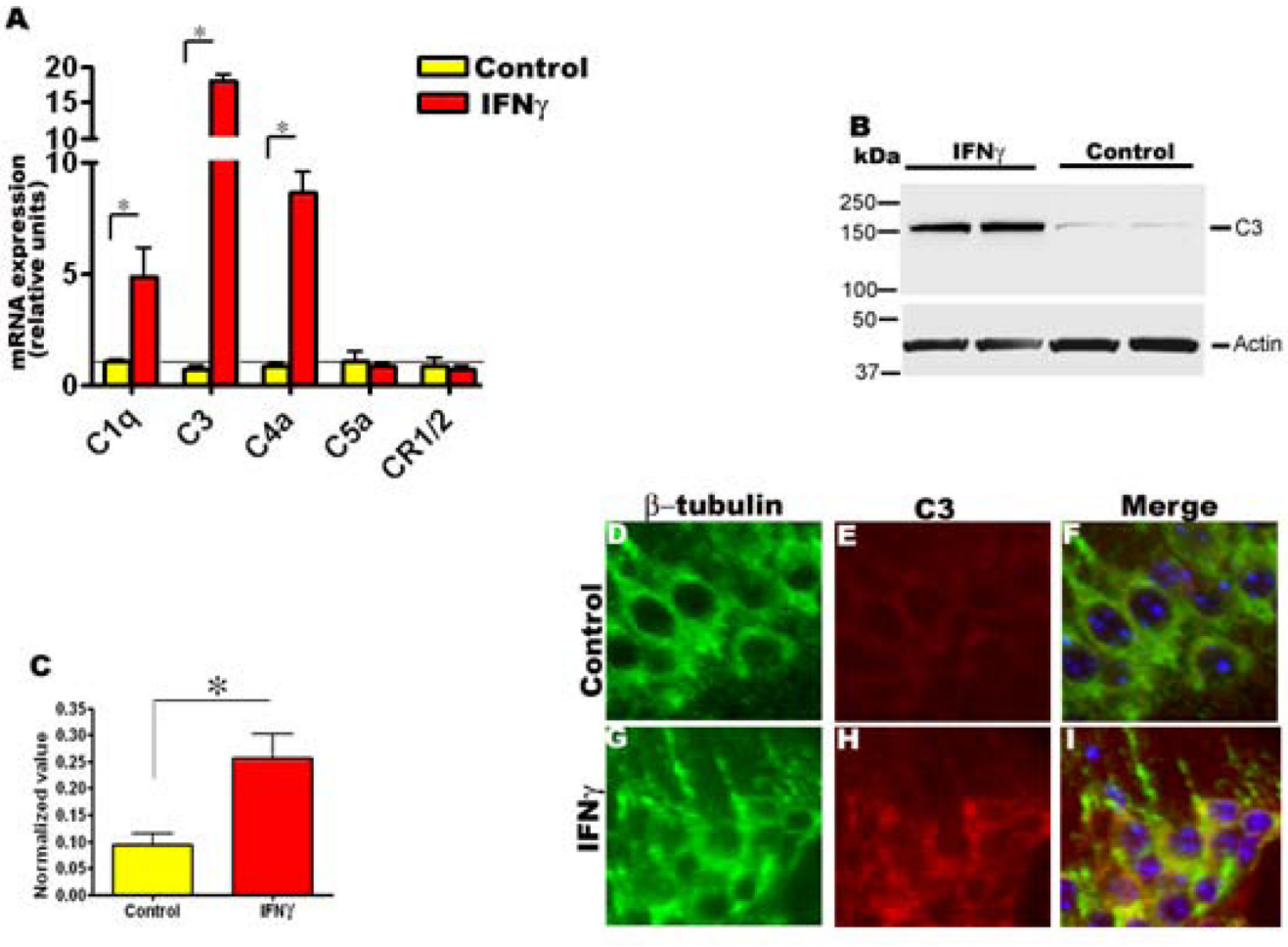

Fig 6. mIFNγ expression leads to increased levels of complement protein C3 in 5 month old TgCRND8 mice

A. Increased mRNA transcript levels of complement protein C1q, C3, and C4a as determined by Q-PCR in P2→5 month old TgCRND8 mice expressing mIFNγ. Relative quantitation of mRNA expression was performed using the comparative cycle threshold method. The expression levels of different genes were normalized using β-actin levels from the corresponding samples. Data, expressed as relative units of mRNA expression, represents averaged fold change values obtained from mIFNγ expressing mice, relative to averaged values obtained from EGFP expressing mice. The horizontal line represents the reference point used for relative mRNA analysis. Error bars indicate SEM. (n=4/group, *p<0.05).

B-C. Representative immunoblot depicting complement C3 protein levels in P2→5 month old TgCRND8 mice expressing mIFNγ or EGFP (B). Quantitative analysis of anti C3 positive immunoreactive band normalized to β-actin shows significantly increased levels of C3 in P2→5 month TgCRND8 mice expressing mIFNγ compared to age-matched controls (C). (n=4/group, *p<0.05).

D-I. Representative images depicting anti-C3 immunofluorescence staining (red stain) colocalizing with β-tubulin immunoreactive neurons (green stain) in the hippocampus of mIFNγ expressing P2→5 month old TgCRND8 mice compared to controls. Blue represents the DAPI stained nuclei. (magnification, 600×). n=3/group.